Characterization of a capillary-discharge plasma

N. Edison,* P. E. Young, N. Holmes, and R. W. Lee
University of California, Lawrence Livermore National Laboratory, Livermore, California 94550

N. C. Woolsey, J. S. Wark, and W. J. Blyth
Department of Physics, Clarendon Laboratory, University of Oxford, Parks Road, Oxford, OX1 3PU, United Kingdom
(Received 10 September 1992)

The electron density and temperature of the plasma produced by a capillary discharge with open geometry have been characterized. Peak densities of 1×10^{19} cm^{-3} and electron temperatures of 2.5 eV are observed. The plasma is uniform over distances on the order of 1 cm. The time evolution of both the electron density and temperature profiles has been studied over the duration of the 5-μs-long discharge.

PACS number(s): 52.25.Rv, 52.40.Nk, 52.50.Dg

I. INTRODUCTION

Capillary-produced plasmas are formed by an electrical discharge through a narrow channel, or capillary, within a solid. The ambient plasmas produced by closed-geometry capillaries, in which the plasma is confined within the solid, typically have densities in the range $10^{19}-10^{22}$ cm^{-3} and temperatures of approximately 2 eV [1], and have been investigated for a number of years due to interest in strongly coupled plasmas. Experimental studies of the standard capillary discharge, however, have been hampered by restricted access to the plasmas. These problems have largely been overcome by the development of the open-geometry form of the discharge to be described below, in which the plasma is allowed to expand into open space away from the solid. This form of discharge presents great advantages in that the ambient plasma can be directly studied, and the plasma can now be laser heated to provide a uniform hot plasma.

In this paper, we describe a series of experiments in which we have directly characterized the time-dependent electron density and temperature profiles of a capillary discharge plasma. Interferometry is used to measure the electron density and optical pyrometry is used to infer the electron temperature profile. The capillary-produced plasma is shown to be extremely uniform with peak densities on the order of 1×10^{19} cm^{-3} and electron temperatures near 2 eV.

Characterization of the electron density of open-geometry capillary plasmas using spectroscopic analysis has been recently presented [2]. Time-integrated observation of Stark line broadening of hydrogen Balmer lines was used to infer plasma densities produced by a polyethylene $[(CH_2)_n]$ insulator. Neither the plasma uniformity nor the electron temperature were investigated. The results of Ref. [2] are consistent with the model of Loeb and Kaplan [3].

Using a capillary discharge, previous workers have produced a large (8.0×0.4 mm^2) plasma which they have laser heated to temperatures of about 250 eV, as indicated by x-ray diagnostics [4]. This earlier work indicated that the plasma might be extremely uniform along the long direction and that the electron density can be varied by changing the electrical energy supplied to the capillary. Although the uniform nature of the plasma has been inferred from spectroscopic measurements and has been simulated with hydrocodes [5], definitive measurements of density and density profiles of the ambient plasma using interferometric techniques have not been applied.

Large uniform plasmas are of great interest because the interpretation of laser-plasma interaction experiments, for example, is often complicated by the nonuniformities of the electron density and temperature of the target plasma. A specific example of this is found in the modeling of x-ray spectra from laser-ablated solids; gradients are inherent to the heating and decompression of the solid target, whether they be in the form of thick microdots, thin embedded microdots, or solid targets [6]. In the case of thick microdots, where the material covers the entire target, the gradients along the axis of the incident laser, i.e., away from the target surface, are large because the material starts at solid density and decompresses into the vacuum. This causes numerous difficulties in the interpretation of the data [7]. In the case of thin dots, which are restricted in both the lateral and horizontal direction there remains the possibility that these dots are hydrodynamically unstable due to the density mismatch between the dot and the surrounding material. Furthermore, the dot generally samples a whole range of densities as it is ablated, and therefore does not constitute a well-defined plasma useful for basic studies of atomic kinetics.

A high-temperature (>1 keV) large plasma could be formed by irradiating a capillary discharge plasma with a high-intensity ($>1\times10^{13}$ W/cm^2) laser beam. Several means of producing large, uniform plasmas have been already investigated, including laser irradiation of exploding foils [8], low-density foams [9,10], and carbon fibers [11]. As noted earlier, laser ablation of solid materials makes it difficult to produce homogeneous plasmas during the laser pulse. Laser irradiation of gas targets have

been performed often in the past, but nonuniformity of the ionization of the gas has been observed [12].

The organization of the remainder of this paper is as follows. We will first describe the capillary and the characterization techniques in Sec. II. The capillary-discharge plasma lifetime is approximately 5 μsec. The density and temperature measurements both have time resolution (<10 ns) within the duration of the discharge lifetime, and both have spatial resolution.

In Sec. III, we will present the data. The emphasis of our discussion will be on the uniformity of the plasma density and temperature. We are able to obtain a plasma which is uniform over millimeter distances. We will also show that the density increase as a function of discharge voltage is less than predicted by theory, while the temperature is independent of the discharge voltage. We conclude by discussing and summarizing the data in Sec. IV.

II. DESCRIPTION OF THE EXPERIMENT

A. The capillary

A schematic diagram of the experimental setup for the capillary-produced plasma is shown in Fig. 1. An insulator [Teflon-$(CF_2)_n$)] separates the anode and the cathode, and has dimensions of 1 cm in diameter by 1 cm high. Within the insulator and the anode there is a 0.2-mm-wide slot, extending through the insulator to the cathode. The slot is tapered in the long dimension, increasing in length from 4 mm next to the cathode to 10 mm at the anode end. The capillary is connected to a 40-μF capacitor which is charged to a selected voltage (≤ 5 kV) that is presently limited by damage to the capillary assembly during a discharge. The discharge is triggered by a 10.0-kV, 35-ns pulse applied between a third electrode (located at the center of the cathode) and the cathode.

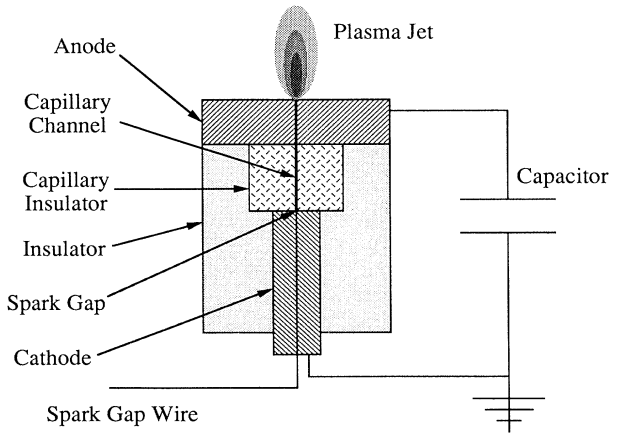

FIG. 1. Schematic of the capillary discharge apparatus. The discharge is initiated by a 10-kV, 30-ns pulse which forms a spark gap with the top of the cathode that is located at the bottom of a 200 μm by 1-cm slot that extends through the Teflon insulator. The discharge occurs between the cathode and the anode through the slot. The plasma ablated from the sides of the slot expands hydrodynamically through a slot in the anode.

The plasma produced in the capillary expands along the gap in the insulator causing ablation of the insulator (Teflon) wall, producing a carbon and fluorine plasma, the density of which can be controlled by the discharge power. The discharge current, which reaches a peak a few microseconds after triggering, is monitored by a Rogowski coil. The plasma expands through the gap in the anode into the surrounding vacuum. The capillary plasma has a lifetime of about 5 μsec.

B. Interferometry

The electron density of the discharge plasma was measured using an interferometer. The plasma was probed using a 2-ns-long laser pulse; before the laser pulse reached the plasma, a fraction of the beam was frequency doubled from a 1.06- to 0.53-μm wavelength by a potassium diphosphate (KDP) crystal, and the two wavelengths propagated colinearly through the plasma. By varying the arrival time of the laser pulse relative to the capillary trigger pulse over many discharges, the time evolution of the density could be studied.

The plasma was imaged using a lens system. The first lens was an $f/4.5$, 240-mm focal length lens that relayed the discharge image through a folded-wave interferometer. In this interferometer scheme, the plasma is offset horizontally relative to the center of the probe beam; a beam splitter picks off a fraction of the beam which is then rotated 180° about a vertical axis through the center of the beam and recombined with the unaltered portion of the beam using a second beamsplitter so that the unobscured portion of the probe beam serves as the reference beam for the portion of the beam occupied by the plasma.

The image formed after the interferometer by the first lens is further magnified by an $f/1.9$, 50-mm lens for a total system magnification of approximately 12 (the resolution is 10 μm in the object plane). The 1.06-μm laser light was imaged onto a charge-coupled-device (CCD) camera, while the 0.53-μm laser light was selected using a narrow-band dielectric mirror and imaged onto film. Recording the two wavelengths simultaneously was important to being able to differentiate between phase shift contributions due to ionized particles and neutral particles (discussed further in Sec. III).

The plasma has an index of refraction $N_p=(1-n_e/n_c)^{1/2}$ where n_e is the electron plasma density and n_c is the critical electron density where the probe laser frequency, ω_0, equals the electron plasma frequency, $\omega_{pe}=(4\pi n_e e^2/m_e)^{1/2}$. The critical density is calculated from $n_c=(1.1\times10^{21})\lambda_L^{-2}$ cm^{-3}, where λ_L is the incident laser wavelength in microns. The plasma produces a phase shift, $\delta\phi$, relative to the reference beam which is given by

$$\delta\phi=(2\pi/\lambda_L)\int_0^L N_p dx$$
$$=(2\pi/\lambda_L)\int_0^L(1-n_e/n_c)^{1/2}dx\ , \quad (1)$$

where L is the path length of the probe beam through the plasma. For $n_e \ll n_c$, this equation is approximated by

$$\delta\phi\approx(\pi/\lambda_L n_c)\int_0^L n_e dx\ . \quad (2)$$

For the experiments reported in this paper, $n_c = 4\times10^{21}$ cm^{-3} for $\lambda_L = 0.53$ μm, whereas the peak density is $n_{e,\text{peak}} = 1\times10^{19}$ cm^{-3}, so the approximation is valid.

Each discharge was probed in one of two directions: along the length of the slot (y direction) or perpendicular to the length of the slot (x direction). (Our coordinate system is defined in Fig. 2.) The path length of the probe beam through the plasma in the y direction is long enough that, at the highest discharge voltages, the density becomes high enough that refraction of the probe beam becomes significant and the fringe shift profile becomes distorted in the z direction near the anode.

An example of the refraction effect is shown in Fig. 3(a) which is an interferogram of the plasma produced by a 2.0-kV discharge as viewed in the y direction. The measurement in the y direction indicates that the plasma density peaks well away (almost 1 mm) from the anode surface whereas the density profile given by the interferogram viewing the perpendicular direction [see Fig. 3(b)] shows that the density profile peaks in the z direction at the anode.

The angle of refraction is given by [13]

$$\theta(z) = (4.5\times10^{-14})\lambda_L^2 \int_0^L \left[\frac{dn_e}{d\mathbf{z}}\right] \times dl \ , \tag{3}$$

where the integral is along the path of the refracted ray and $\mathbf{z}$ is in the direction normal to the surface of the anode slot. The path length of the probe propagating along the length of the slot is so long that even modest density gradients can produce significant refraction. For $\lambda_L = 1.06$ μm, $L = 1$ cm, and $dn_e/d\mathbf{z} = 2\times10^{20}$ cm^{-4} [from Fig. 4(b)], then $\theta \approx 6°$ which is consistent with the deflection of rays from the anode surface to 1 mm away at the end of the plasma. The focusing lens compensates to a certain extent for the refracted rays, however, its effect is limited because the object's extent is much larger than the depth of focus of the lens.

Refraction is not important when the plasma is viewed in the x direction because the path length through the plasma is much shorter. The fringe shift becomes small, however, when the discharge voltage is low, or at early times during the discharge. In these cases, we use the y-direction view to obtain the density profile; the effect of refraction in this case is tolerable. Since the refraction is strongly dependent on the probe wavelength, we also used the interferogram formed by the 0.53-μm probe beam (the 1.06-μm interferogram is shown in Fig. 3).

Discharges at the higher energies (3–5 kV) showed evidence of the presence of a measureable density of neutral particles, which give rise to fringes shifting in the direction opposite to that produced by the plasma electrons. The plasma index of refraction is always less than 1, while the index of refraction of the neutral gas is always greater than 1. The neutral density (in cm^{-3}) is found from the fringe shift, N_n, by

$$n_n = -\frac{N_n\lambda_p}{2\pi\alpha L} = (-1.6\times10^{23})N_n\lambda_p/L \ , \tag{4}$$

which has been found using the Lorentz-Lorenz relation

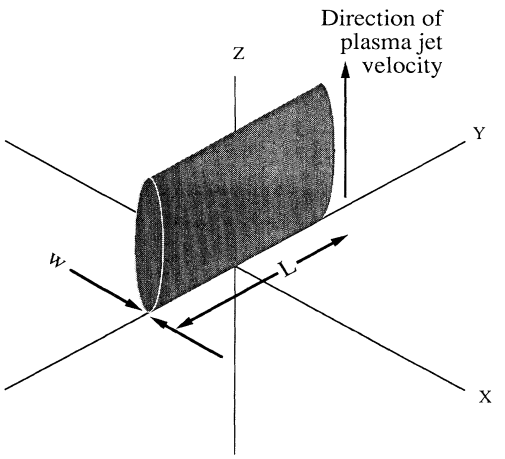

FIG. 2. Coordinate system used for the discussion in the text. The y axis is parallel to the long dimension of the slot in the capillary anode, the x axis is perpendicular to the slot, and the z axis is normal to the anode surface.

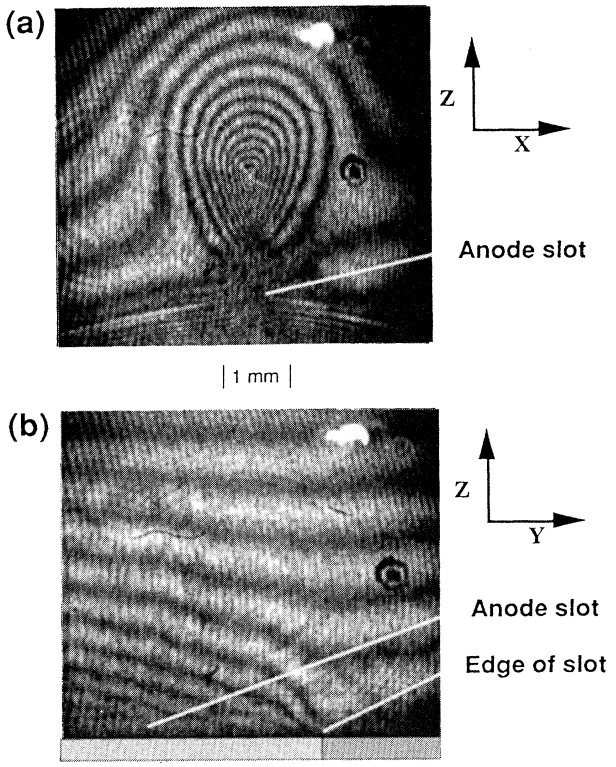

FIG. 3. Interferograms obtained from a capillary discharge with a charging voltage of 3.2 kV. The anode slit width is 375 μm and the interferograms are taken 5 μsec after the discharge is triggered. The probe wavelength is 1.06 μm. The interferograms were acquired on different discharges with views (a) along the y axis and (b) along the x axis.

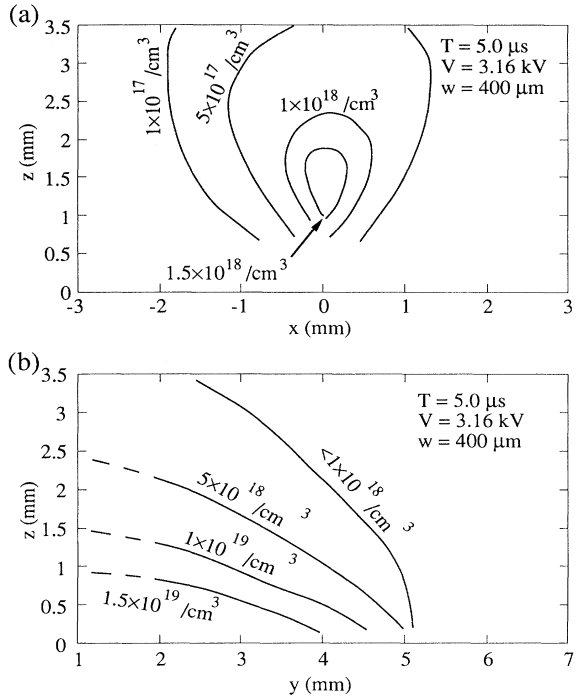

FIG. 4. Density distributions calculated from the interferograms of Fig. 3. The density appears to peak away from the anode in the z direction because of refraction of the probe beam (discussed in the text).

[14] where α is the atomic polarizability, and we have used the measured polarizability for a 1:2 carbon-fluorine atomic gas [15]. The indices of refraction for the plasma and the neutral gas also have a different dependence on the probe wavelength; this means that by looking simultaneously at interferograms produced at two different probe wavelengths, it is possible to deconvolve the separate contributions of the plasma and the neutral gas. In all cases, the neutral contribution was small (apparently limited to the ends of the slot) being within the measurement and superposition error. We will show, in Sec. III C, that the measured neutral density is consistent with the measured plasma temperature.

Once the interferograms have been obtained, the density distribution is calculated using Eq. (2) and an assumption that the density is uniform along the line of sight. The density distributions obtained from the interferograms of Fig. 3 are shown in Fig. 4.

C. Pyrometry

In the setup for the pyrometry measurement, which provides an indication of temperature, a lens ($f/10$, focal length is 50 cm) images the plasma source through an interference filter onto an optical fiber bundle. For all the data discussed, the plasma was viewed in the x direction. The fiber bundle transmits the plasma light to six photomultiplier tubes. Each photomultiplier time resolves a spot size of ≈ 500 μm in diameter [16] to obtain a spatial profile of the plasma emission. The spectrum is resolved by changing the center wavelength of the interference filter during the experiment while keeping the external parameters of the discharge constant. The time response of the photomultiplier is ~ 2 ns.

The plasma temperature was inferred by comparing the spectral surface luminosity of the plasma to a standard source. The standard source in this case was a tungsten lamp with a helical filament ($T \approx 2800$ K at 35 A); the luminosity of this lamp is referenced to a National Bureau of Standards (now NIST) calibration. Between the wavelengths of 400 and 700 nm, the filament was found to emit a spectrum which matches that of a blackbody radiator:

$$I_{\text{cal}}(\lambda, T_0) = 2\pi a_0 hc^2/\lambda^5 [\exp(hc/\lambda k T_0) - 1] , \quad (5)$$

where I_{cal} is the calibrated intensity, $a_0 = 0.448 \pm 0.016$ is the calibration emissivity, and $T_0 = 3231 \pm 18$ K is the calibration source temperature. The spectral radiance of the lamp at $\lambda = 550$ nm is 200 W/m^2 nm sr.

The observed plasma emission intensity, I_{plasma}, is related to the plasma temperature by

$$\frac{I_{\text{plasma}}}{I_{\text{cal}}} = \frac{A}{a_0} \frac{\exp(h\nu/kT_0) - 1}{\exp(h\nu/kT) - 1} , \quad (6)$$

where ν is the frequency of the emitted light, and A is the plasma absorption. The plasma absorption is introduced because the plasma is optically thin ($A \ll 1$). The plasma emission along the line of sight, therefore, contributes to the signal produced by the photomultiplier tube. This also means that A is a function of T so the calculation of T from I_{plasma} is an iterative procedure (discussed further in Sec. III B).

III. RESULTS

The capillary discharge was investigated by varying the discharge voltage, and the width of the slit in the anode. In this section, we discuss data using discharge voltages

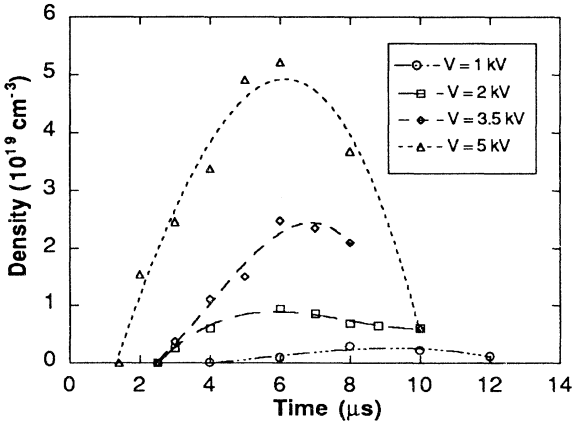

FIG. 5. Peak density vs time for a slot width of 200 μm. Discharges produced by four different charging voltages were studied. The data points have been fitted with a third-order polynomial.

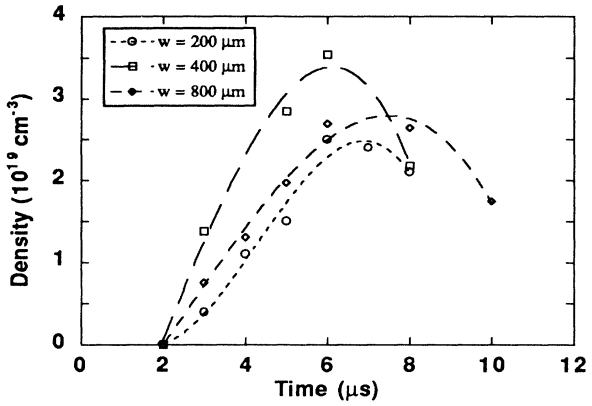

FIG. 6. Peak density vs time for a 186-J discharge energy (3.2-kV charging voltage) and three different anode slot widths.

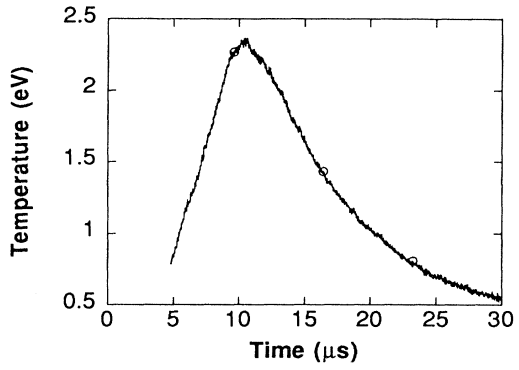

FIG. 7. Temperature variation as a function of time. The light is collected from a region in the middle of the slot, 325 μm above the anode. The discharge energy is 18.6 J (1-kV charging voltage).

of 1, 2, 3, and 5 kV, and slot widths of 200, 400, and 800 μm. The behavior of the plasma as a function of time and space was also studied.

A. Density measurements

The experiments show that the peak density scales linearly with the discharge energy. Figure 5 shows that the density peaks approximately 5 μsec after the discharge is triggered, regardless of the charging voltage, which coincides with the time of peak current passing through the capillary.

The peak density is independent of the width of the slot in the anode. In Fig. 6, we show the time history of the plasma density as the slot width is increased from 200 to 800 μm. This result shows that the anode contributes little to the total plasma density and that we should expect little variation in the peak density as long as the width of the Teflon slot remains constant.

The optimized capillary produces peak densities of 1×10^{19} cm^{-3}. The plasma is also extremely uniform over a large volume. Figure 4(b), for example, shows that the plasma density varies less than a factor of 3 for $0.5<z<1.5$ mm and $|y|<4$ mm.

B. Temperature measurements

The plasma is optically thin at 530 nm as shown in the interferograms by the transmission of the probe beam. This means that [17]

$$A=1-e^{-\tau}, \tag{7}$$

where

$$\tau=\int_0^L \mu\, dx \tag{8}$$

and [18]

$$\mu=\frac{16\pi^2e^6Z^2kT_en_e}{3\sqrt{3}h^4c\nu^3}\exp\left[-\left[\frac{I-h\nu}{kT}\right]\right]. \tag{9}$$

We use Z as the charge state, ν as the emission frequency, and I is the emissivity at frequency ν. The expression for μ includes bound-free and free-free transitions. We obtain n_e from the density measurement, so T_e is the only quantity needed to calculate μ and A. This requires an iterative solution of Eq. (6) for T given n_e and I.

We assume that the emissivity is constant throughout the discharge and calculate A using the peak density and iteratively solve Eq. (6) for T_e. The results for a discharge of 1 kV with a peak density of 2.5×10^{18} cm^{-3} give $T_e=2$ eV and $A=0.0041$.

The time-dependent temperature is plotted in Fig. 7. In calculating the temperature, we have assumed that the absorption is constant for a given discharge and equal to the value of the absorption at the peak density of the discharge. To test this approximation, we calculated the time-dependent absorption and found the results in agreement within 20%.

Our measurements of the neutral density are consistent with that predicted by the Saha equation using our measured electron temperature. For a discharge voltage of 3.5 kV, we can place an upper bound on the neutral density of 10^{19} cm^{-3}. Since this discharge produces a peak electron density of 3×10^{19} cm^{-3}, the average ionization is greater than 75%. For the measured electron density,

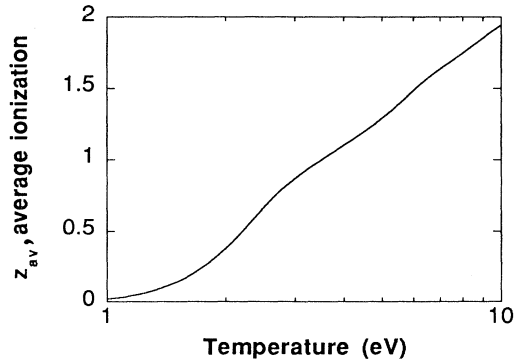

FIG. 8. Plot of the average ionization, z_{av}, as a function of temperature of a plasma containing a 1:2 ratio of carbon and fluorine atoms.

and assuming a 1:2 ratio of carbon and fluorine atoms, the Saha prediction of ionization as a function of temperature is shown in Fig. 8. The estimate of 75% ionization places a lower bound on the temperature of 2.7 eV, in good agreement with the measured peak temperature of 2.5 eV.

C. Discussion of the data

To summarize the data, we have found the following: (i) The peak electron temperature is independent of the discharge energy. (ii) The time of the peak temperature relative to the discharge trigger varies, however, and occurs earlier as the discharge voltage is increased. (iii) Regardless of the height above the anode, the electron temperature is extremely uniform along the length of the plasma, as shown in Fig. 9. We see that T_e is uniform within 50% over a distance of approximately 1 cm.

The observed density and temperature distributions are the result of the physical processes involved in the formation of the plasma within the capillary channel, the geometry of the capillary channel, and the expansion of the plasma into the vacuum. The current, voltage, and power in the capillary channel as a function of time for a discharge voltage of 1 kV are shown in Fig. 10(a). The current is uniform within 10% for nearly a 5-μsec duration. The peak density as a function of time is compared to the capillary power in Fig. 10(b). It can be seen that the time between the triggering of the spark gap and the first appearance of a plasma at the output of the capillary is approximately 4 μsec. Since the capillary is 1 cm high, this corresponds to a velocity at the capillary output of 2.5×10^5 cm/sec, in good agreement with the velocity measured from the expansion rate of the electron density profile. This expansion velocity is also in good agreement with the plasma sound velocity calculated from the measured peak electron temperature of 2.3 eV. The time-dependent electron temperature is shown for comparison in Fig. 10(c).

During the time when the current is nearly constant (for $3<t<6$ μsec in Fig. 10), the capillary discharge is in quasisteady state since the rate of change of the current is much slower than the hydrodynamic time scale ($l/c_s \leq 2$ μs). The measured resistivity agrees well with Spitzer's resistivity for a fully ionized plasma [2,19]:

$$R = 0.17(l/a^2)(\ln\Lambda)/T^{3/2}\ , \tag{10}$$

provided we replace the dimension a, which is the diameter of the capillary opening in the cylindrical geometry of the theory, with the diameter that gives an area equal to that of the slotted capillary of our experiment. The measured resistivity for a 1-kV discharge is $R=0.5$ kV/2.25 kA$=0.22$ Ω. For this discharge, we measured $T=2$ eV, and $n=5\times10^{18}$ cm^{-3}, so $\ln\Lambda\sim2$. The capillary depth, l, was 1 cm, and $a=0.7$ mm, so $R=0.24$ Ω, in good agree-

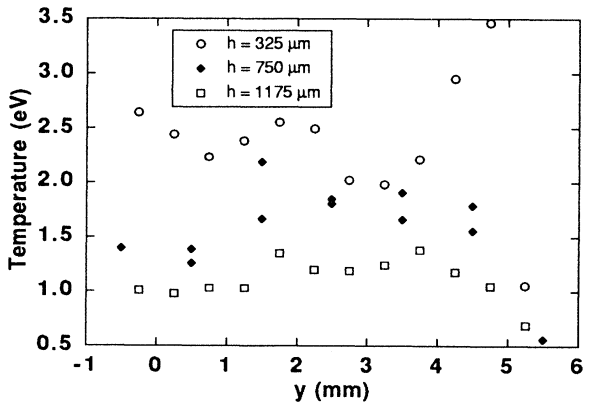

FIG. 9. Temperature variation along the slot for three different distances above the anode. Each data point is the average of six consecutive shots. The charging voltage was kept constant at 2.0 kV.

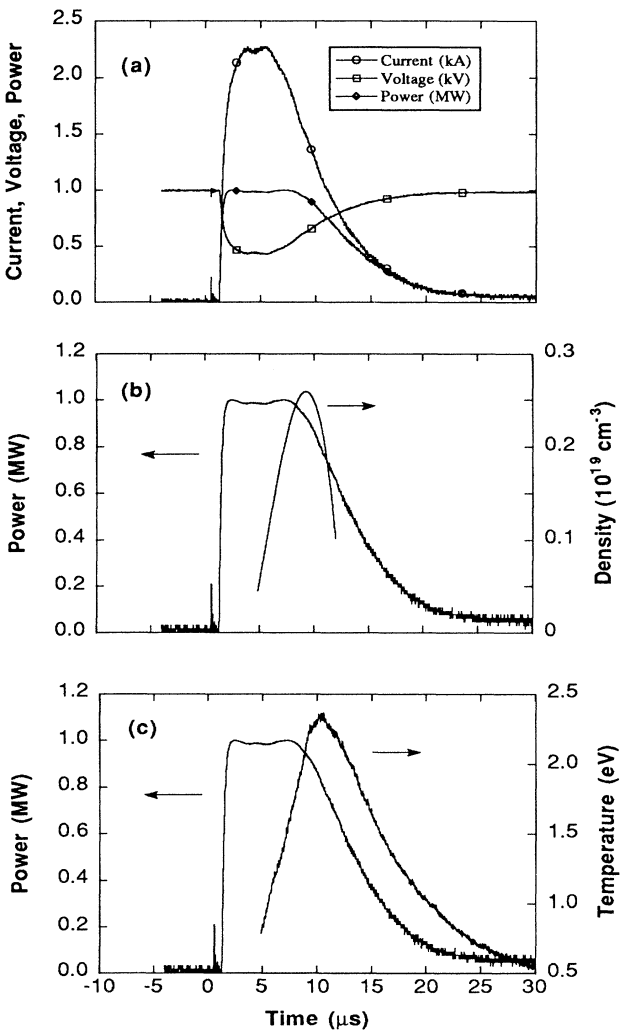

FIG. 10. Comparison of external electrical properties of the discharge with the measured peak density and temperature for a discharge voltage of 1 kV. (a) Plot of the time-dependent current (kA), voltage (kV), and power (MW). (b) Plot of the time-dependent power and the time-dependent density. (c) Plot of the time-dependent power and the time-dependent temperature.

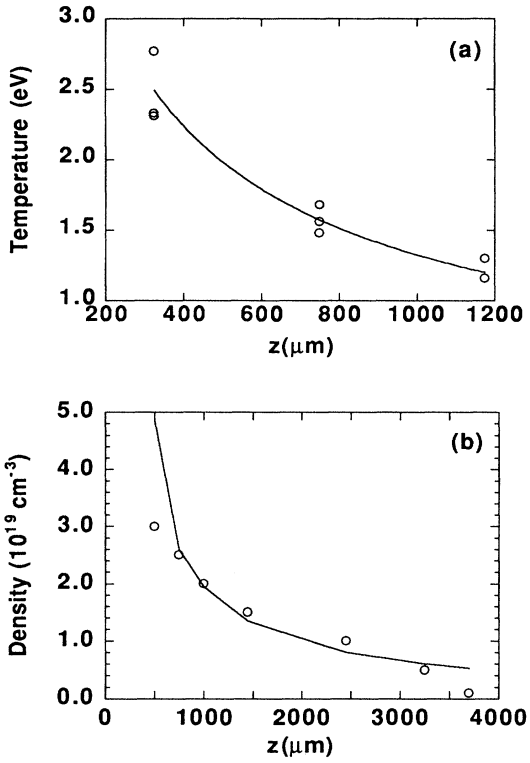

FIG. 11. Comparison of the observed temperature and density profiles for a 3.2-kV discharge with the profiles calculated for an adiabatic plasma expansion. Shown are (a) temperature and (b) density profiles at the time at which the density peaks.

ment with the resistivity measured from the external currents.

We compared our observed scaling of peak density and temperature with the model of Loeb and Kaplan [3]. Using Eq. (29) of Ref. [3] and Ohm's law, $T_e \propto V_c^{4/5}$ is predicted, whereas we observe no change in T_e with the discharge voltage, V_c. Similarly, the model predicts $n_e \propto V_c^2$ [from Eq. (31) of Ref. [3]]; in the experiment the peak density is proportional to V_c. The difference between our experiment and the prediction is probably due to the breakdown of the assumption in the model of an optically thick plasma. As we have seen, the plasma is optically thin, and probably also is so inside the capillary: the plasma absorption, A, will be less than 1 even if the density is an order of magnitude larger inside the capillary than outside. The low density, and resistivity, observed in this experiment are the result of the large cross-sectional area of the slotted capillary compared to the cylindrical capillary of the model.

The observed temperature and density profiles agree well with those predicted by an adiabatic expression of the plasma in the vacuum. The temperature, T, plasma volume, V, and pressure, $P = nT$, are related by

$$V^{\gamma-1}T = \text{const} ,$$

$$TP^{(1-\gamma)/\gamma} = \text{const} .$$

Above the capillary, the plasma expands horizontally at the sound speed, so $V \propto z$, $T \propto z^{-2/3}$, and $n \propto z^{-1}$. Comparison of this formulation with the data (see Fig. 11) shows good agreement. A model in which the plasma expansion is driven by a constant source [20] predicts that the density should fall an order of magnitude over the same axial distance shown in Fig. 11.

IV. CONCLUSIONS

We have measured the time-resolved densities and temperatures of an open-geometry capillary-discharge plasma. Peak densities of 3×10^{19} cm^{-3} and temperatures of 2.5 eV have been obtained. The measured density and temperature profiles show a plasma that is uniform over millimeter distances.

The time-resolved measurements show the relationship between the discharge current and the evolution of the temperature profile. Steady-state flow of the plasma has been obtained in the discharge examined here. The large aperture of our capillary produces a somewhat lower plasma resistivity than has been previously investigated.

The large ion densities inferred from our measurements lead to the prediction of high electron densities ($> 10^{20}$ cm^{-3}) if a high-intensity laser beam is used to fully ionize the target plasma [5]. The result will be a plasma which includes the density ranges seen in laser-ablated plasmas from solid targets, but uniform over a much larger size, and with significantly lower (by two orders of magnitude) hydrodynamic flow. For the production of long scale length uniform plasmas, the slotted capillary discharge provides a promising source for a wide variety of interesting plasma studies.

ACKNOWLEDGMENTS

We thank A. Zigler for the early design of the discharge apparatus used in this experiment. This work was performed under the auspices of the U.S. Department of Energy by the Lawrence Livermore National Laboratory under Contract No. W-7405-Eng-48.

*Present address: Laboratoire de Physique des Milieux Ioniés, Ecole Polytechnique, 91128 Palaiseau CEDEX, France.

[1] S. M. Zakharov, A. A. Kolomenskii, S. A. Pikuz, and A. I. Samokhin, Pis'ma Zh. Tekh. Fiz. **6**, 1135 (1980) [Sov. Tech. Phys. Lett. **6**, 486 (1980)].

[2] J. Ashkenazy, R. Kipper, and M. Caner, Phys. Rev. A **43**, 5568 (1991).

[3] A. Loeb and Z. Kaplan, IEEE Trans. Magn. **25**, 342 (1989).

[4] A. Zigler, M. Kishenevsky, M. Givon, E. Yarkoni, and B. Arad, Phys. Rev. A **35**, 4446 (1987).

[5] L. B. Petway, C. A. Back, K. Estabrook, R. W. Lee, and A. Zigler, J. Appl. Phys. **66**, 1632 (1989).

[6] R. L. Kaufmann, R. W. Lee, and K. Estabrook, Phys. Rev. A **35**, 4286 (1987).

[7] D. Duston, J. Davis, and P. C. Kepple, Phys. Rev. A **24**, 1505 (1981); M. J. Herbst, P. G. Burkhalter, R. R. Whitlock, J. Grun, and M. Fink, NRL Memorandum Report No. 4812, 1982 (unpublished).
[8] D. L. Matthews, P. L. Hagelstein, M. D. Rosen, M. J. Eckart, N. M. Ceglio, A. U. Hazi, H. Medecki, B. J. MacGowan, J. E. Trebes, B. L. Whitten, E. M. Campbell, C. W. Hatcher, A. M. Hawryluk, R. L. Kauffman, L. D. Pleasance, G. Rambach, J. H. Scofield, G. Stone, and T. A. Weaver, Phys. Rev. Lett. **54**, 110 (1985).
[9] K. A. Tanaka, B. Boswell, R. S. Craxton, L. M. Goldman, F. Guglielmi, W. Seka, R. W. Short, and J. M. Soures, Phys. Fluids **28**, 2910 (1985).
[10] H. Figeroa, C. Joshi, and C. E. Clayton, Phys. Fluids **30**, 586 (1987).
[11] D. Jacoby, G. J. Pert, S. A. Ramsden, L. D. Shorrock, and G. J. Tallents, Opt. Commun. **37**, 193 (1981).
[12] J. E. Bernard and J. Meyer, Phys. Fluids **29**, 2313 (1986).
[13] F. C. Jahoda and G. A. Sawyer, in *Methods of Experimental Physics: Plasma Physics, Part B,* edited by R. H. Lovberg and H. R. Griem (Academic, New York, 1971).
[14] J. D. Jackson, *Classical Electrodynamics* (Wiley, New York, 1975), p. 155.
[15] *CRC Handbook of Chemistry and Physics,* 67th ed. (CRC, Cleveland, 1986), pp. E67 and 68.
[16] H. B. Radousky and A. C. Mitchell, Rev. Sci. Instrum. **60**, 3707 (1989).
[17] Ya. B. Zel'dovich and Yu. P. Raizer, in *Physics of Shock Waves and High Temperature Hydrodynamic Phenomena,* edited by W. D. Hayes and R. F. Probstein (Academic, New York, 1966), p. 110.
[18] Ya. B. Zel'dovich and Yu. P. Raizer, in *Physics of Shock Waves and High Temperature Hydrodynamic Processes* (Ref. [17]), p. 271.
[19] L. Spitzer, *Physics of Fully Ionized Gases* (Interscience, New York, 1962).
[20] A. V. Farnsworth, Jr., M. M. Widner, M. J. Clauser, P. J. McDaniel, and K. E. Lonngren, Phys. Fluids **22**, 859 (1979).

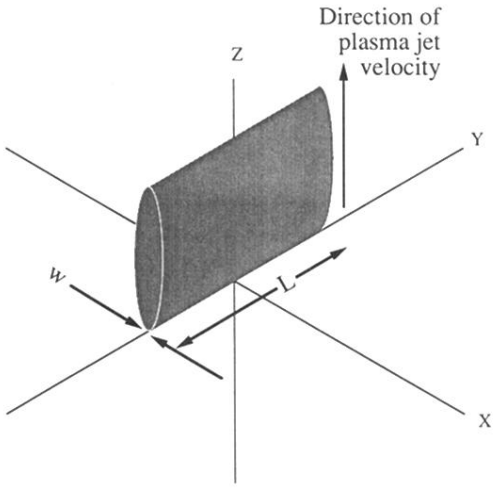

FIG. 2. Coordinate system used for the discussion in the text. The y axis is parallel to the long dimension of the slot in the capillary anode, the x axis is perpendicular to the slot, and the z axis is normal to the anode surface.

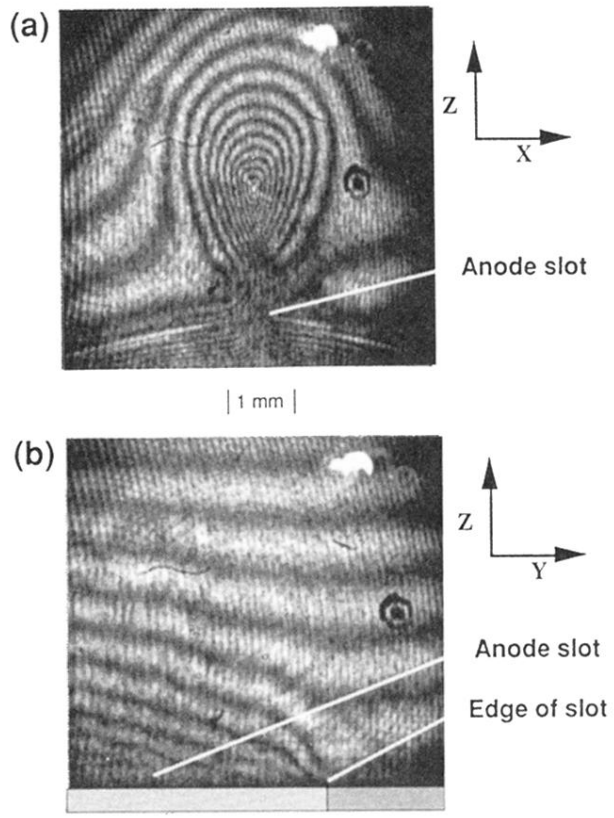

FIG. 3. Interferograms obtained from a capillary discharge with a charging voltage of 3.2 kV. The anode slit width is 375 μm and the interferograms are taken 5 μsec after the discharge is triggered. The probe wavelength is 1.06 μm. The interferograms were acquired on different discharges with views (a) along the y axis and (b) along the x axis.